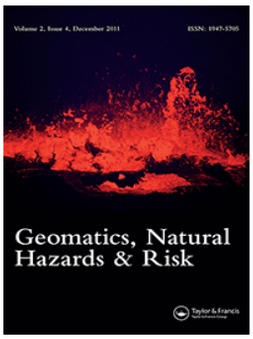

Geomatics, Natural Hazards and Risk

ISSN: (Print) (Online) Journal homepage: www.tandfonline.com/journals/tgnh20

Monitoring of post-fire forest scars in Serbia based on satellite Sentinel-2 data

Olga Brovkina, Marko Stojanović, Slobodan Milanović, Iscander Latypov, Nenad Marković & Emil Cienciala

To cite this article: Olga Brovkina, Marko Stojanović, Slobodan Milanović, Iscander Latypov, Nenad Marković & Emil Cienciala (2020) Monitoring of post-fire forest scars in Serbia based on satellite Sentinel-2 data, Geomatics, Natural Hazards and Risk, 11:1, 2315-2339, DOI: 10.1080/19475705.2020.1836037

To link to this article: https://doi.org/10.1080/19475705.2020.1836037

Published online: 09 Nov 2020.

GEOMATICS, NATURAL HAZARDS AND RISK
2020, VOL. 11, NO. 1, 2315–2339
https://doi.org/10.1080/19475705.2020.1836037

Taylor & Francis
Taylor & Francis Group

Monitoring of post-fire forest scars in Serbia based on satellite Sentinel-2 data

Olga Brovkina[a], Marko Stojanović[a], Slobodan Milanović[b], Iscander Latypov[c], Nenad Marković[d] and Emil Cienciala[a,e]

[a]Global Change Research Institute of the Czech Academy of Sciences, Brno, Czech Republic; [b]Chair of Forest Protection, Faculty of Forestry, University of Belgrade, Belgrade, Serbia; [c]Saint-Petersburg Scientific Research Centre for Ecological Safety, RAS, St. Petersburg, Russia; [d]State Enterprise "Srbijašume", Belgrade, Serbia; [e]IFER – Institute of Forest Ecosystem Research, Jilove u Prahy, Czech Republic

ABSTRACT

This study aims to improving long-term post-fire environment assessment. It proposes a method for monitoring fire impact using Sentinel-2 satellite data by combining spectral and textural features of land cover types inside a post-fire study sites. Specific objectives were to 1) test stability of the burnt area index for Sentinel-2 (BAIS2) for identification of burn in study sites, 2) investigate the optimal feature combination for mapping land covers inside study sites, and 3) assess and analyse dynamic in land covers of study sites. BAIS2 was shown independent on date acquisition of satellite images to distinguish forest burn from other land covers over the analysed May–September vegetation period. Texture of study site improved the classification results. The most accurate classification method for identification of study sites land covers (with 0.84 Kappa coefficient and 0.86 overall accuracy) was based on combination of Sentinel-2 bands, BAIS2, and texture by Fourier transform. Analysis of vegetation recovery within the study sites demonstrated different recovery rates. Natural regeneration of pine was not observed, during three to six years of observations following fire events. The proposed method and findings can support planning of forest management measures needed to effectively restore forest cover.

ARTICLE HISTORY
Received 9 July 2020
Accepted 8 October 2020

KEYWORDS
Forest burn; classification; recovery; image texture; BAIS2; spectral analysis

1. Introduction

Forest fires constitute natural and inevitable process. More than 65,000 wildfires occur annually in Europe, burning an area of some half-million hectares (San-Miguel-Ayanz et al. 2019). In recent decades, the severity and frequency of forest fires has increased along with total area burned (Moreira 2012). In Southern Europe, the major reasons related to fire regime changes lies in socio-economic changes occurring after World War II linked to land abandonment and afforestation of previously

CONTACT Olga Brovkina brovkina.o@czechglobe.cz

agricultural land. That caused more fuel accumulation and landscape-level connectivity of flammable parcels (Moreira 2012). In addition to land cover changes, the altered fire regime can be attributed also to increased temperature and shifted precipitation patterns (hotter and drier summer periods) caused by climate changes (Moriondo et al. 2006; Koutsias et al. 2013). According to Turco et al. (Turco et al. 2014), it can be expected that fire severity will increase particularly in Mediterranean countries, including the Balkans (Radovanovic et al. 2015).

In Serbia, forest fires constitute one of the worst forms of ecosystem damage to forests and one of the major challenges for forest management (Milanovic 2019). In the past decade, the area burnt per year has markedly increased, 42.3% increase in 2000s as compared to 1990s (International Forest Fires News (IFFN); Lukić et al. 2017). In the period from 2012 to 2016 alone, 414 forest fires were registered and accounted for burnt area totalling more than 9,428 ha with average size of 25.6 ha (min: 0.01; max 1383.14, StDev: 104.76 ha) (Marčeta and Milanović 2018). Data collection concerning area burned by forest fires is provided only for state-owned forest, however, and not for privately owned forest (Aleksić et al. 2009), even though the latter accounts for more than 1 million hectares and 47% of total forested area (Banković et al. 2008). Likewise, the surface areas affected by forest fires are estimated either subjectively according to the size of the affected forest unit or by GPS devices (Milanovic 2019). Consequently, forest fires occurring in Serbia may be severely underreported. Meanwhile, post-fire revitalization of forest ecosystem is costly, and these sites are often left to natural regeneration (Ratknić 2017). In order to monitor burnt forest areas and forest recovery patterns, remote sensing methods can be applied and validated with measures being from field observations.

Mapping and modelling complex post-fire forest patterns and their changes over time comprise a key issue in spatial forest ecology that is related to fire (Teodoro and Amaral 2019). In recent decades, satellite optical remote sensing techniques increasingly have been applied to monitoring of burnt forest areas in order to map vegetation changes (Milne 1986), measure burn severity (White et al. 1996), estimate degree of post-fire vegetation changes (Lentile et al. 2006), and explore recovery time point in relation to post-fire processes (Ryu et al. 2018). In studies of post-fire effects, burnt area mapping is one of the most common applications of satellite optical remote sensing, and it is well documented at local, regional, and global levels (Chu et al. 2013). Satellite remote sensing methods used to map post-fire patterns are based on supervised classification (Kontoes et al. 2009), object-based classification (Polychronaki and Gitas 2010; Mencuccini and Christoffersen 2019), analysis of single spectral indices (Huang et al. 2016), multitemporal series of spectral indices (Filipponi 2019), linear transformations (Patterson and Yool 1998), and spectral unmixing procedure (Meng et al. 2017). Assessment of ecological responses (e.g. vegetation recovery) as part of burn-severity analysis is also studied in part using remote sensing. The tools used most frequently for analysing and mapping the temporal and spatial dynamics of post-fire environments are vegetation indices (Cuevas-Gonzalez et al. 2009; Morresi et al. 2019) and products derived from them (Veraverbeke et al. 2012). These advanced approaches have been applied mostly to Landsat Thematic Mapper (TM)/Enhanced Thematic Mapper (ETM) imagery, which combines 30 m spatial resolution and 16-day revisiting time and is regarded as the

most valuable source of time-series data at a landscape scale – long temporal record of Landsat from 1982 to present (Banskota et al. 2014; Vogelmann et al. 2016).

Over the past few years, progress has been achieved in identifying burnt forest areas based on multispectral satellite Sentinel-2 (S2) data. In comparison to Landsat, S2 has increased multispectral bands (with three unique red edge wavelengths), 20 m spatial resolution (multispectral bands), and revisit period as short as 5 days. S2 red-edge spectral indices (Modified Simple Ratio, Chlorophyll Index, Normalized Difference Vegetation Index) have been applied for discriminating four burn-severity levels after wildfire (Fernández-Manso et al. 2016). To differentiate between burnt and unburnt areas, S2 bands (short and long shortwave infrared [SWIR] bands b11 and b12) and spectral indices (Mid-Infrared Burnt Index (MIRBI) and Normalized Burnt Ratio 2 [NBR2]) have been examined and found to have the highest separability index values (Huang et al. 2016; Roteta et al. 2019). A newly developed burnt area index for S2 (BAIS2) has been presented to detect burnt areas and perform post-fire mapping (Filipponi 2018). Potentially, these can distinguish S2 data as one of the most powerful sources of information to discriminate vegetation components of burnt areas and estimate their changes over time.

Although multispectral satellite data have been used actively in monitoring fire burning, assessing suitable remote sensing data and methods for characterizing burnt forest areas and evaluating their recovery dynamics were not fully explored (Ryu et al. 2018). This study is directed to improving long-term post-fire environment assessment. It proposes an original method for monitoring of damaged by fire forest sites using Sentinel-2 satellite data. The method combines spectral and textural features of land cover types inside post-fire study sites. Specific objectives are to 1) test stability of the burnt area index for Sentinel-2 (BAIS2) for identification of burn in study sites, 2) investigate the optimal feature combination for mapping land covers inside study sites, and 3) assess and analyse dynamic in land covers of study sites.

2. Materials and methods

2.1. Study area

Four post-fire sites, which are selected for the study, are situated in the central part of Serbia (Figure 1). Three sites (1–3) had previously been covered by artificially established coniferous forest and the fourth was a natural beech forest. The forest fires occurred on study sites from 2007 to 2015 (Tab 1). After fire, study sites have been cleaned by cutting the remaining trees that were significantly damaged by fire. Foresters did reforestation with pine seedlings which was not successful and spontaneous vegetation started to occupy burned and cleaned areas. The different temporal scale was important for this study to estimate recovery after longer time periods since forest fire occurred. Beside the conifer forests (sites 1-3) we were interested to test the recovery dynamics in broadleaf forest (site 4). Succession stage of the study sites can be described as a stage of intermediate species (Figure 2), where grasses, shrubs and young deciduous are presented.

The sites varied in age from 20 to 50 years at the time of fire and ranged in altitude from 440 to 750 m a.s.l. The sites are exposed to the sun for most of the day.

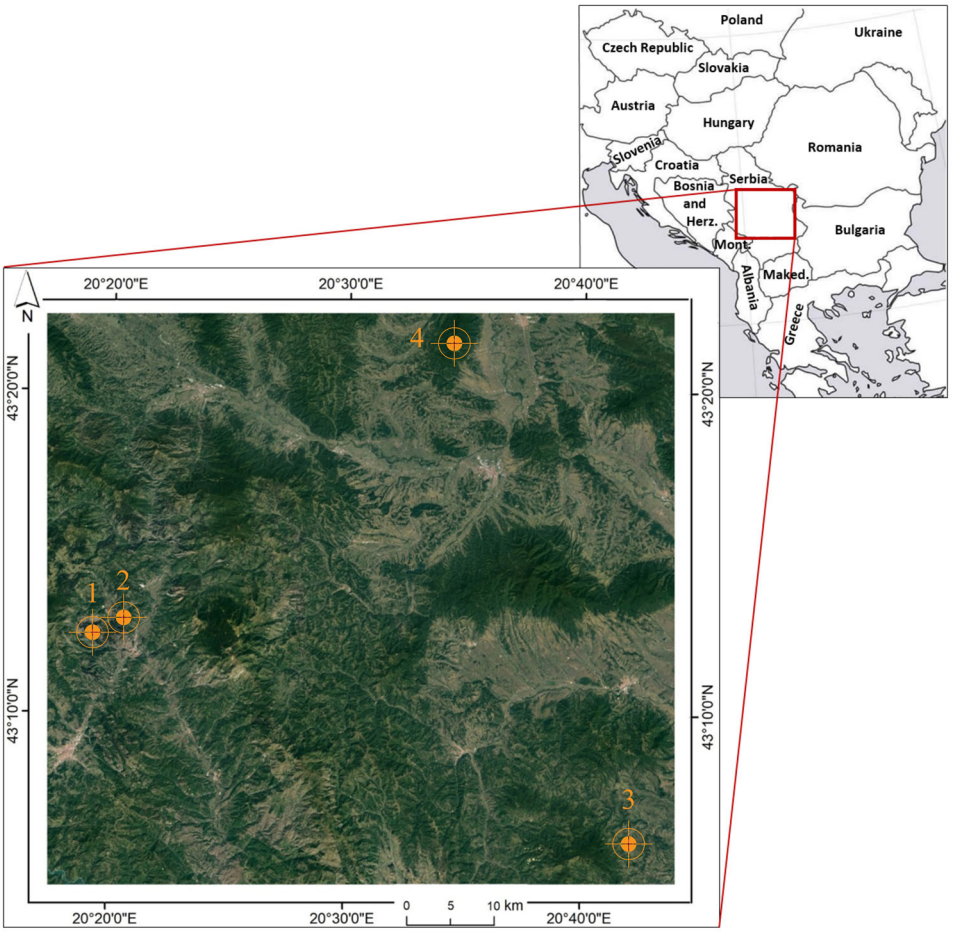

Figure 1. Study area. Orange marks show location of study sites. Background is Sentinel-2 image displayed in true color.

Average temperature and precipitation totals for the fire season (March-October) at study sites are presented in Table 1. Borders of study sites were outlined based on archival forest inventory materials and GoogleEarth satellite images before and after fire. To assess the likely fire intensity on the study sites, we used fire danger class. It was categorized based on fire weather index (FWI (Dowdy et al. 2009),) calculated after the fire. FWI has 6 categories: very low (FWI $<$ 5.2), low (5.2 $\leq$ FWI $<$ 11.2), moderate (11.2 $\leq$ FWI $<$ 21.3), high (21.3 $\leq$ FWI $<$ 38), very high (38 $\leq$ FWI $<$ 50) and extreme (FWI $\geq$ 50). FWI values for our study sites corresponded to moderate, high and very high fire danger class (Table 1).

2.2. Field data

Fieldwork was conducted during May–June 2019. It involved identifying land cover types on four study sites: charring and sparse grass cover, charring and dense grass cover, small bushes with charring, bushes with young broadleaf trees, forest (Figure 3a). At

Table 1. Characteristics of study sites.

Site no.	Forest type before fire	Age of forest, years	Altitude [m], aspect	Temperature [°C]/ Precipitation [mm]*	Date of fire dd.mm.yy	Burnt area [ha]	Fire danger class (FWI)**	Forest type after fire	Dates of Sentinel-2 images for analysis
1	Coniferous – Austrian pine plantation	20	600–620 flat	15.1/405	08.08.2012	24.0	Very high (47.5)	Broadleaf – oak stand	05.08.2016 16.06.2016 11.07.2017 14.09.2017 27.05.2018 21.07.2018 10.08.2018 10.09.2018 11.06.2019
2	Coniferous – Austrian pine plantation	25	550–750 SW-SE	13.9/424	01.05.2012	188.5	Moderate (12)	Broadleaf – oak stand	15.08.2016 11.07.2017 30.08.2017 19.09.2017 21.07.2018 18.08.2019 10.08.2019
3	Coniferous –Austrian pine plantation	20	625–825 S	11.9/702	05.09.2015	42.5	High (24.7)	Broadleaf – oak stand	15.08.2016 11.07.2017 30.08.2017 19.09.2017 21.07.2018 18.08.2019 10.08.2019
4	Broadleaf – beech forest with small enclaves of Austrian pine	50	440–720 E	12.0/697	27.07.2007	82.7	High (33.9)	Broadleaf – beech stand	05.08.2016 11.07.2017 05.08.2017 27.05.2018 10.08.2018 11.06.2011 10.08.2019

*Average air temperature [°C] and precipitation [mm] totals for the fire season (March-October) for 1979-2013 period were obtained from the Climate Forecast System Reanalysis (CFSR, https://globalweather.tamu.edu).

**Fire ganger class categorizes based on fire weather index (FWI) which has 6 categories: very low (FWI < 5.2), low ($5.2 \leq$ FWI < 11.2), moderate ($11.2 \leq$ FWI < 21.3), high ($21.3 \leq$ FWI < 38), very high ($38 \leq$ FWI < 50) and extreme (FWI ≥ 50).

each selected location, at least one georeferenced picture was taken for each cardinal point (North, East, South, and West). The pictures were used for assigning training and validation samples for further satellite image classification (Table 2). Training samples were used for model construction in classification process. Where each sample of the training set was annotated with it's appropriate class. Validation samples were used to validate the classification accuracy.

2.3. Satellite Sentinel-2 imagery data

Satellite S2 imagery data (15 scenes) were downloaded from the Sentinels scientific data hub (https://scihub.copernicus.eu/). Date of scenes are presented in Table 1. Satellite S2 10 spectral bands were used in the study: B2 (0.490 μm), B3 (0.560 μm), B4 (0.665 μm), B5 (705 μm), B6 (0.740 μm), B7 (0.783 μm), B8 (842 μm), B8A (0.865 μm), B11 (1610 μm) and B12 (2.190 μm). Scenes from 2017, 2018 and 2019 were available for downloading with processed Level-2A (bottom-of-atmosphere-reflectance), and scenes from 2016 were downloaded with processed Level-1C (top-of-atmosphere-reflectance). Reformatting of Level-1C data to Level-2A data was performed in Sen2Cor processor (Main-Knorn et al. 2017).

2.4. Burned Area Index for Sentinel-2

Burned Area Index for Sentinel-2 (BAIS2) was used to identify charring on study sites. It was computed for each study site and each S2 scene according to the following formula (Filipponi 2018):

$$BAIS2 = \left(1 - \sqrt{\frac{B6 * B7 * B8A}{B4}}\right) * \left(\frac{B12 - B8A}{\sqrt{B12} + B8A} + 1\right), \quad (1)$$

where B4 (0.665 μm), B6 (0.740 μm), B7 (0.783 μm), B8A (0.865 μm) and B12 (2.190 μm) are spectral bands of S2 image.

Vegetation indices differ greatly in terms of their sensitivity to various external factors. This may affect the spectral reflectance signatures of objects on the image and the classification results. To avoid potential misclassification when using BAIS2 to identify charring on study site, the index was tested for sensitivity to vegetation period of satellite data acquisition. In our case, BAIS2 was tested to identify 'charring and sparse grass' cover on study sites. BAIS2 was calculated for each S2 satellite scene through the May–September vegetation period. Second coefficients in Chebyshev polynomials of the first kind (Mason and Handscomb 2002) were derived from the set of BAIS2 values from May to September for study site land covers: charring and sparse grass cover, charring and dense grass cover, small bushes with charring, bushes with young broadleaf trees, forest, and artificial object (road). Differences between the second coefficients in Chebyshev polynomials of land covers were examined using statistical t-test.

BAIS2 was used as an input for automatic classification of study sites as a feature to identify 'charring and sparse grass' class.

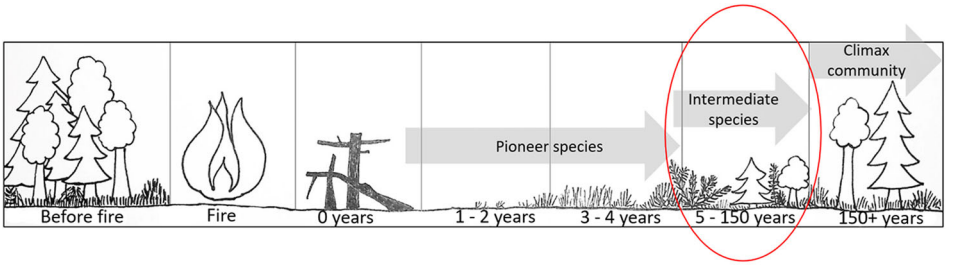

Figure 2. Succession stages after fire. Succession stage of the study sites is marked in red.

2.5. Texture analysis

The use of textural information in image classification, apart from spectral data, can significantly increase the accuracy of classification (Haralick et al. 1973). The best results can be obtained by using a combination of spectral and textural data (Bekkari et al. 2012; Kupidura 2019). Texture can be a distinctive feature of selected land cover classes exhibiting significant spectral similarities. It has no unambiguous definition (Bracewell 2000), which is why in the practice of digital image processing many different methods of texture analysis have been defined. For this study, Fourier transform (Kupidura 2019) and computation of image statistics were applied for texture characterizations of study sites.

Fourier transform is valuable for analysing the repetitive structure of image objects (Gonzales and Woods 1992; Proisy et al. 2007). Fourier transform converts an image into a two-dimensional function with two frequency components (horizontal and vertical). Once the transformation is applied, the Fourier spectra define the image by their components of phase and amplitude. A moving window is used to compute the filtered values (i.e. components of phase and amplitude) for each pixel. In this study, the optimal window size for Fourier transformation of S2 data was determined to be 16×16 pixels, that allowed identify basic texture elements, textels, of study site land covers. Three coefficients of Fourier transform were selected from 16×16 possible coefficients to characterize texture of study sites. These were: maximum amplitude, where amplitude is the length of the complex vector; and two amplitudes of the 1^{st} coefficient and 10^{th} coefficient adjacent to the central one shifted by unity in Y and in X, respectively. The maximum amplitude specified the difference between intensity values. Amplitudes of the 1^{st} coefficient and 10^{th} coefficient were degrees of 'blurring' on the image texture. The 'soft' texture values might help to avoid misclassification when texture and spectral features are together in image classification process.

S2 red edge spectral band (B6, 0.740 µm) was used in the texture analysis, because spectral reflectance of land covers had a maximum difference in the spectral region 0.740.0.865 µm (Figure 3b). The texture is formed by alternation of the grey scale in the spatial position, such that there is a certain spatial relationship between two pixels separated by a certain distance within the image. The statistical method included the calculation of dispersion, percentile, and autocorrelation within each study site. The metrics analysed the relationship between pixel pairs considering that each pixel (except for those on the periphery of an image) had eight neighbouring pixels. Dispersion described how spread out a pixel values were. Percentiles corresponded

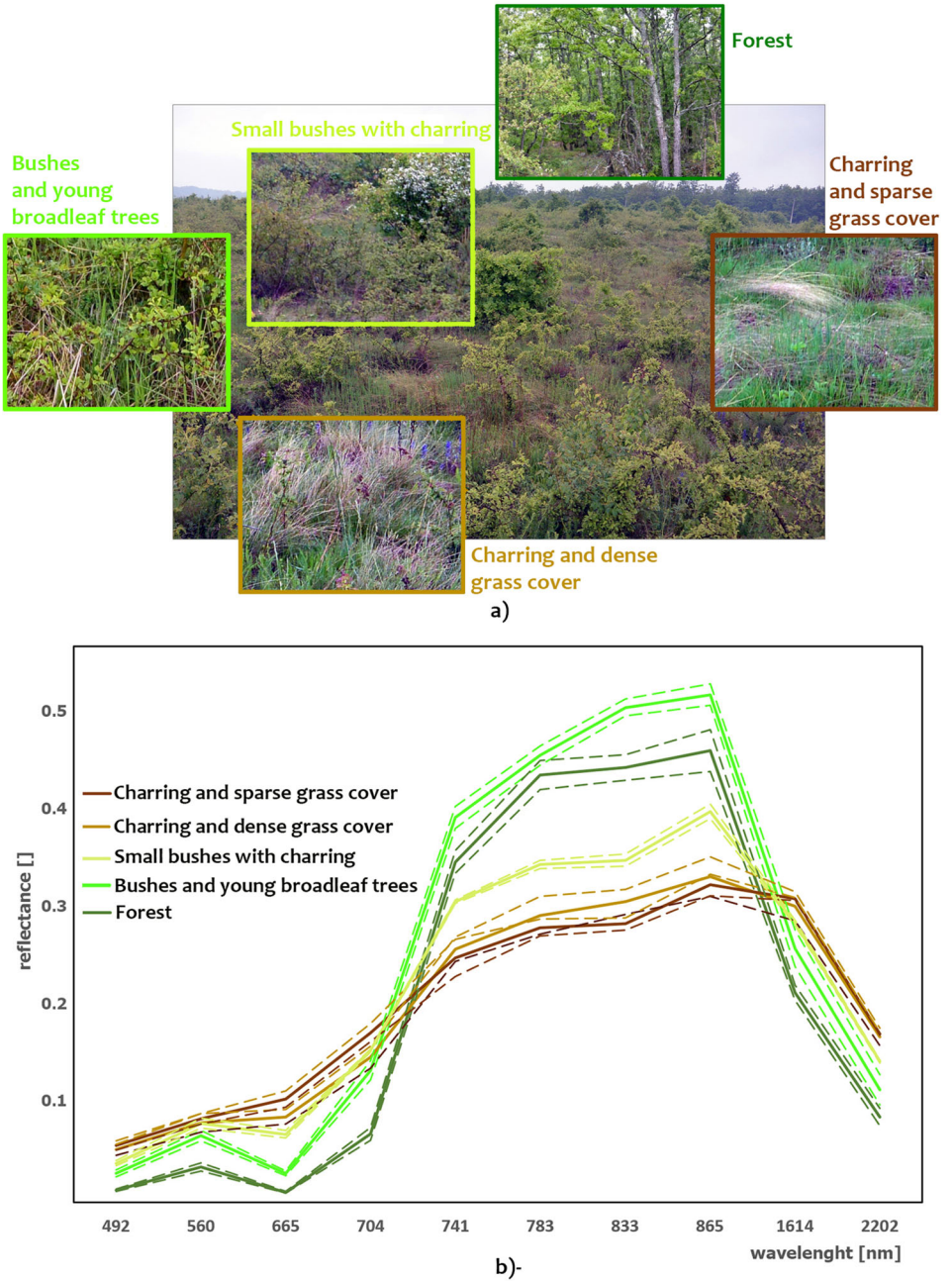

Figure 3. Study site 1: a) Ground truth pictures, b) Spectra of study area land covers extracted from Sentinel-2 data. Continues line refers to mean reflectance, dotted lines show the range of reflectance values from all class samples for each land cover class.

within the distribution of pixel values on the image. In our case, the 5th percentile was a value associated with the location within the data where 5% of data was below that value. It was scaled with respect to the original image and allows simultaneous

Table 2. Training and validation samples from fieldwork for study sites classification based on Sentinel-2 data.

	Study site land covers					
Samples	Small bushes with charring	Bushes with young broadleaf trees	Charring with sparse grass cover	Charring with dense grass cover	Forest mixed *	Forest broadleaf
Training	10	8	6	8	5	4
Validation	8	6	3	6	3	2
Study site	1, 2, 3, 4	2, 3, 4	1, 2, 3, 4	1, 2, 3, 4	1, 2, 4	4

*Forest mixed is broadleaf forest with small mixture of conifers.

analysis of small and large texture elements, textels. Autocorrelation function in image analysis was used for recognition of textels or textel boundaries.

Computation and visualization of texture features was performed with specific program code, written by the paper authors. Visualizations of texture features for study site 1 is presented in Figure 4. The texture features were used as an input for automatic classification of study sites.

2.6. Classification of study sites

Classification steps are demonstrated on flow chart (Figure 5). Support vector machine (SVM) classifier implemented in EnMAP-box plug-in (van der Linden et al. 2015) was applied in the study. The algorithm is based on statistical learning theories where a linear discriminant function is established by constructing the classification surface to ensure the maximum distance between the samples (Cristianini and Shawe-Taylor 2000).

We used four sets of features as classification inputs to classify study sites:

- S2 bands (hereinafter, bands 2, 3, 4, 5, 6, 7, 8a, 11, 12),
- S2 bands with BAIS2,
- S2 bands with BAIS2 and texture by Fourier transform, and
- S2 bands with BAIS2 and texture by image statistic computation.

To compare classification results from four sets of features, Kappa coefficient and overall classification accuracy were computed. To classify study sites for 2016, 2017 and 2018 we used a set of features that demonstrated the most accurate classification results from 2019. Due to the lack of field data for 2016, 2017 and 2018, the reliability of classification referring to 2016, 2017 and 2018 years was estimated based on analysis of spectral signatures of each class on the original image. Spectral similarity algorithm was used for scenes from 2016, 2017 and 2018 to detect occurrence of the reference spectra signatures. The algorithm compared spectra of classes from 2016, 2017 and 2018 with reference spectra from 2019.The output of the algorithm was a ranked score for each of the reference spectra from 1 to 0, where 1 indicated the closest match and indicated higher confidence in the spectral similarity. To estimate reliability of classification from 2016, 2017 and 2018 the reference spectra score of 0.8 and higher was considered.

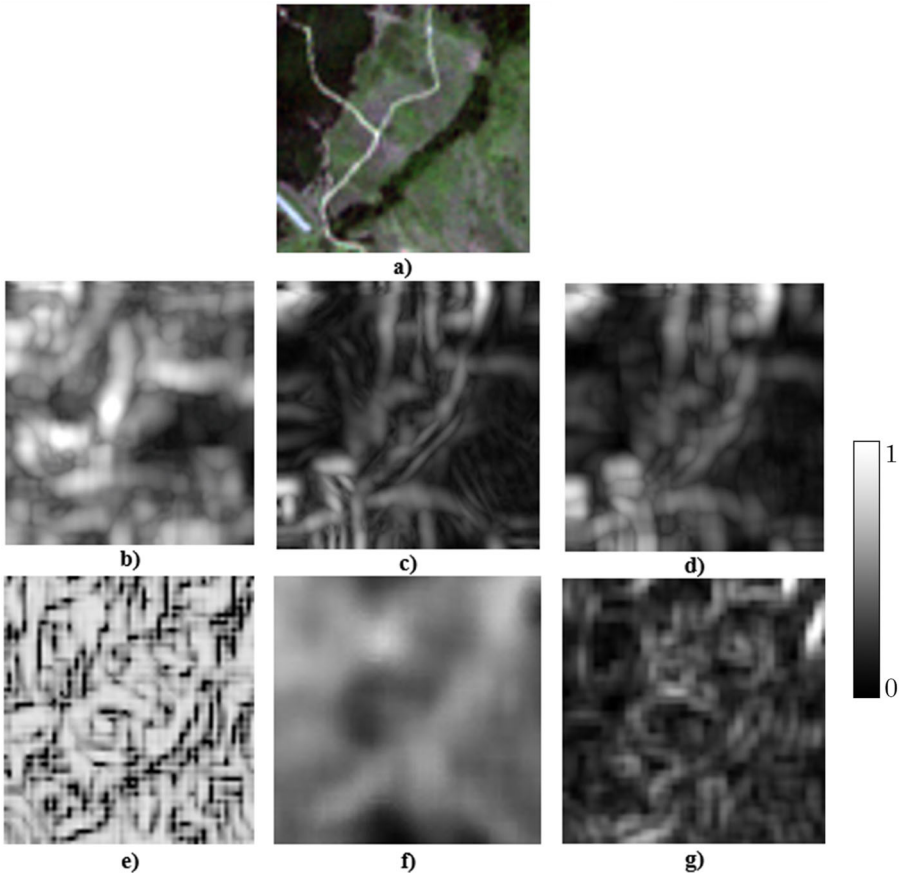

Figure 4. Visualizations of texture features for study site 1: a) red–green–blue (RGB) Sentinel-2 data; Fourier transform coefficients as b) maximum amplitude, c) 1st coefficient, and d) 10th coefficient; and image statistics as e) autocorrelation, f) percentile, and g) dispersion. Scale of values for texture features is from 0 to 1.

2.7. Dynamic in study sites land covers

Dynamics in study sites land covers were calculated using percentage of each class from classification result for 2016, 2017, 2018 and 2019. The Change function was used to enumerate the differences between two classified raster datasets for land cover change analysis in geographic information system. Relative difference computation method was applied. We used pair of classified raster: 2016 and 2017, 2017 and 2018, 2018 and 2019. The output raster datasets contained values with 'no change' (0) and 'change' (all other values) for each compared pair.

3. Results

3.1. Spectra analysis of study sites

The spectra of study sites land covers were analysed using the reference spectra of undamaged forest stands in the spectral interval of 0.492–2.202 μm. There was a marked reduction in near-infrared surface reflectance and rise in visible surface

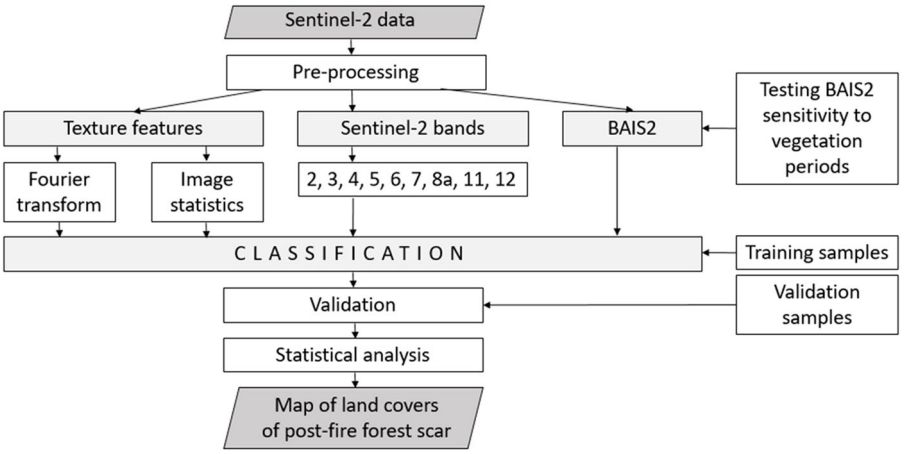

Figure 5. Flow chart of classification steps.

reflectance in land covers with mixtures of charring and dense grass cover, charring and sparse grass cover, and small bushes with charring (Figure 3b).

3.2. BAIS2 stability across the vegetation period

Analysis of the second coefficient of Chebyshev polynomials $T_2\ (x)$ of BAIS2 for main land covers (charring with sparse grass cover, charring with dense grass cover, small bushes with charring, bushes and young broadleaf trees, forest, and road) on the S2 satellite scenes showed that differences between $T_2\ (x)$ of charring with sparse grass cover and $T_2\ (x)$ of other land covers were statistically significant for the May–September vegetation period (p-values ranged from 0.004 to 0.008, $\alpha = 0.01$) (Table 3). BAIS2 demonstrated a stable identification of charring on all analyzed satellite scenes acquired in various dates of vegetation period.

3.3. Classification of study sites

Study sites were classified into four (study sites 1, 3), five (study site 2) and six classes (study site 4). Each site contained classes of: charring and sparse grass cover, charring and dense grass cover, small bushes with charring. Forest cover was identified in study sites 1, 2 and 4. Study site 4 had two forest classes: broadleaved (beech) and mixture (beech with small enclaves of pine) (Figures 6–9). Confusion matrix of classified land cover types demonstrates true classes (columns) and classifier predictions (Table 4). The diagonal elements (bold values) represent the number of points for which the predicted label is equal to the true label, while off-diagonal elements are those that are mislabeled by the classifier. A notable misclassification belong to the classes - charring and sparse grass cover, and charring and dense grass cover – which were classified one as another (about 16%) on study sites 2, 3 and 4. Forest (about 20%) was misclassified with class of small bushes with charring on study site 2. Other classes had high true positive rate with misclassification no more than 6%. Overall classification accuracy and Kappa coefficient for four classification inputs and for each study site are shown in Table 5.

Table 3. Second coefficient of Chebyshev polynomials for post-fire forest scar land covers.

	Image land cover					
	Charring and sparse grass cover	Charring and dense grass cover	Small bushes with charring	Forest	Bushes and young broadleaf trees	Road
T_2 (x)*	−0.08	−0.07	−0.11	−0.28	−0.32	−0.06
p-value	–	0.0091	0.008	0.004	0.004	0.0003

T_2 (x) is second coefficient of Chebyshev polynomials of the first kind. P-value is a result of a statistical t-test: differences between T_2 (x) of charring with sparse grass cover and T_2 (x) of other land covers.

The most accurate classification result for study site 1 was distinguished when the classification input contained S2 bands and BAIS2. The most accurate classification results for study sites 2 and 3 were distinguished when the classification input contained a texture by Fourier transform. Overall accuracy (0.78) and Kappa (0.77) were the same when the classification input contained S2 bands with BAIS2 and a texture by Fourier transform for study site 4. Classification with S2 bands, BAIS2 and texture by statistics demonstrated less accurate overall accuracy and Kappa coefficient for all study sites than classification with texture by Fourier transform.

Within 4 years of observations, vegetation dynamic were detected for all study sites (Figure 10). The coniferous plantations (sites 1, 2, 3) showed insignificant or absent (site 3) recovery of Austrian pine, the dominant species prior to the fire event. Instead, the recovery was generally dominated by other vegetation classes, with a specific intensity apparently related to time since the fire event and extent of the fire.

4. Discussion

4.1. Spectra analysis of study sites

When vegetation is burnt, there is a drastic reduction in visible-to-near-infrared surface reflectance (i.e. 0.4–1.3 µm) that is associated with the charring and removal of vegetation (Eva and Lambin 1998; Cristianini and Shawe-Taylor 2000). The spectra land covers with mixtures of charring and dense grass cover, charring and sparse grass cover, and small bushes with charring in our study have markedly lower reflectance in the near-infrared part of the electromagnetic spectrum (0.72–1.3 µm) compared to land covers of bushes with young broadleaf trees, and forest. Charring and dense grass cover, charring and sparse grass cover, and small bushes with charring are characterized by gradual reflectance increase in the 0.5–0.7 µm part of the electromagnetic spectrum, whereas common vegetation spectra fluctuate up and go down within this part of the electromagnetic spectrum. Variation in spectral response of study sites land covers can be explained as a function of burn severity (White et al. 1996). The larger the difference in spectra of land covers within a burnt area, the greater the difference in fire damage.

4.2. BAIS2 stability

Analysis of BAIS2 for land covers of study sites showed that BAIS2 can differentiate class charring with sparse and dense grass cover from other land covers through the

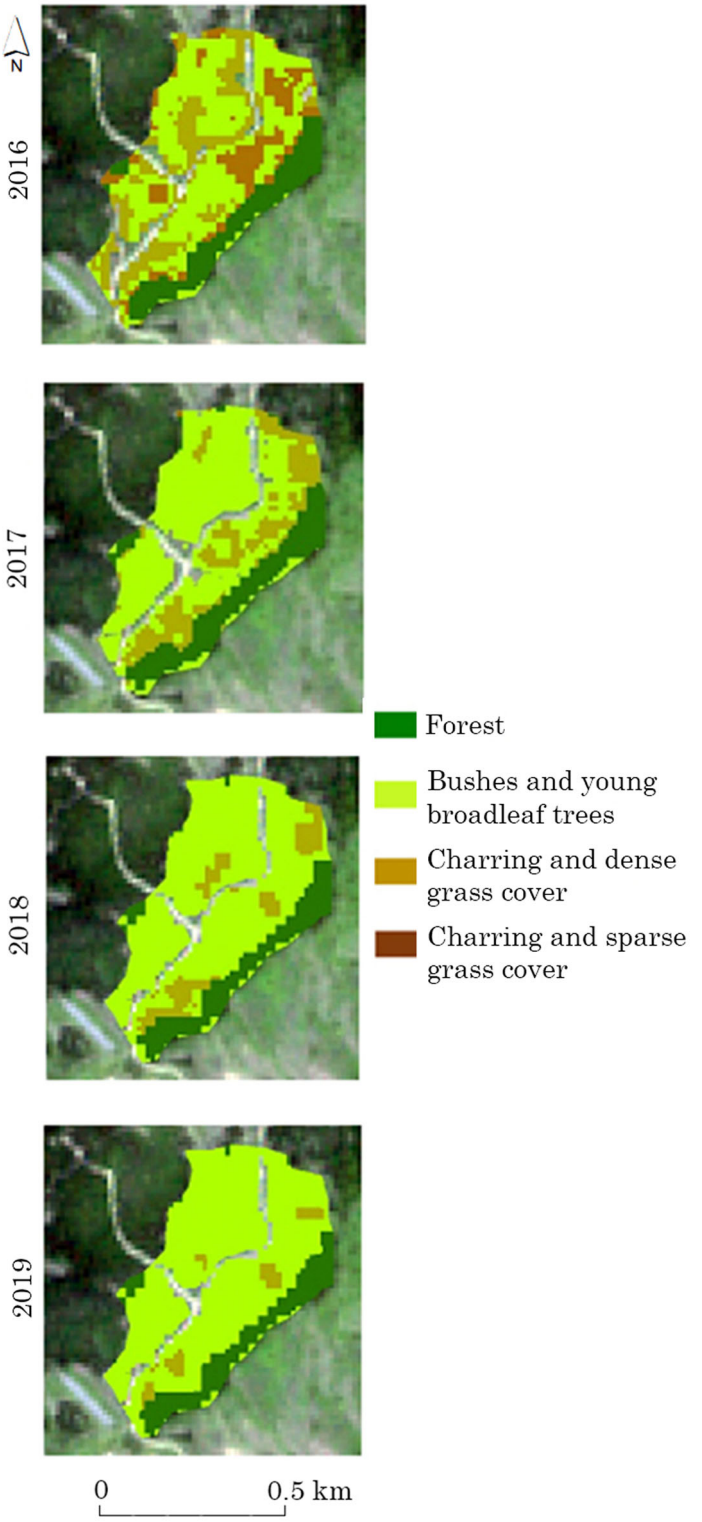

Figure 6. Classification results for study site 1.

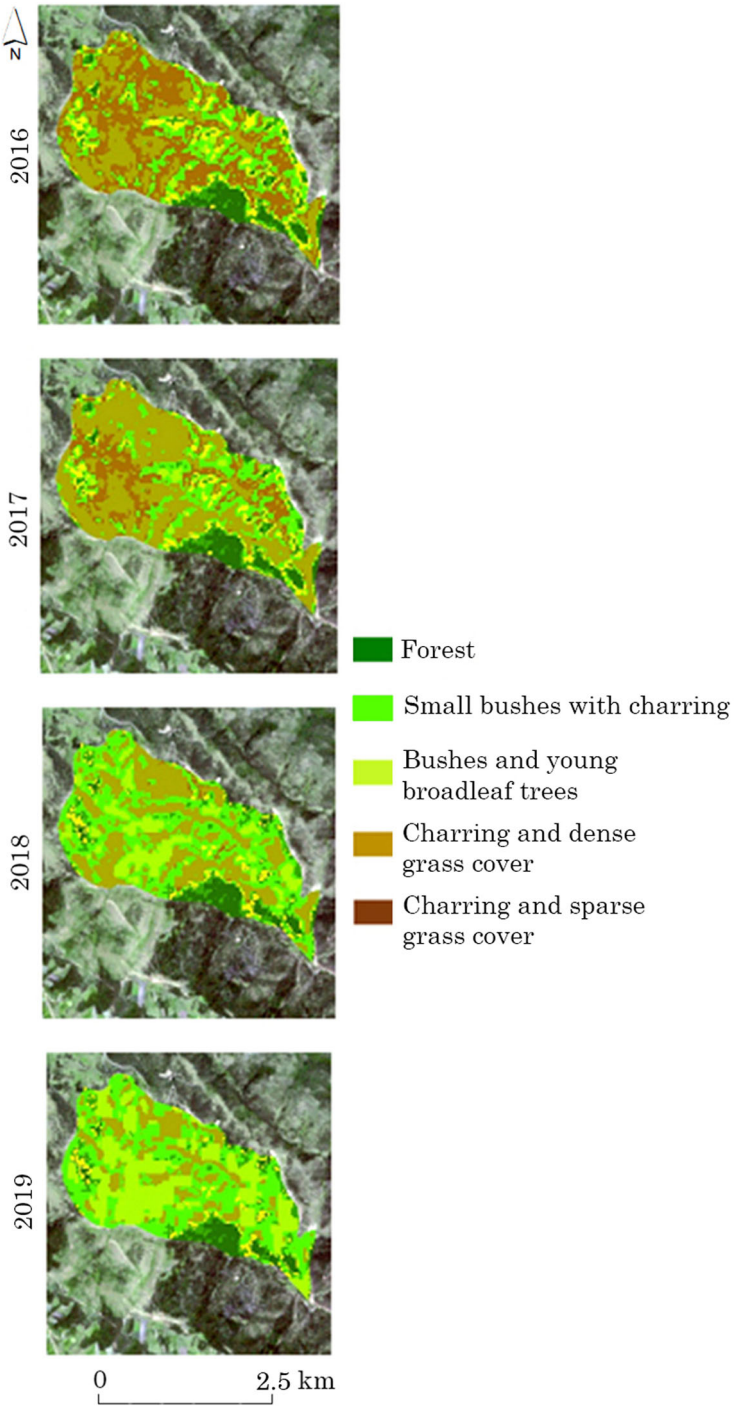

Figure 7. Classification results for study site 2.

analyzed May–September vegetation period. Our BAIS2 results complement the existing findings from testing of widely used vegetation indices for their burn detection

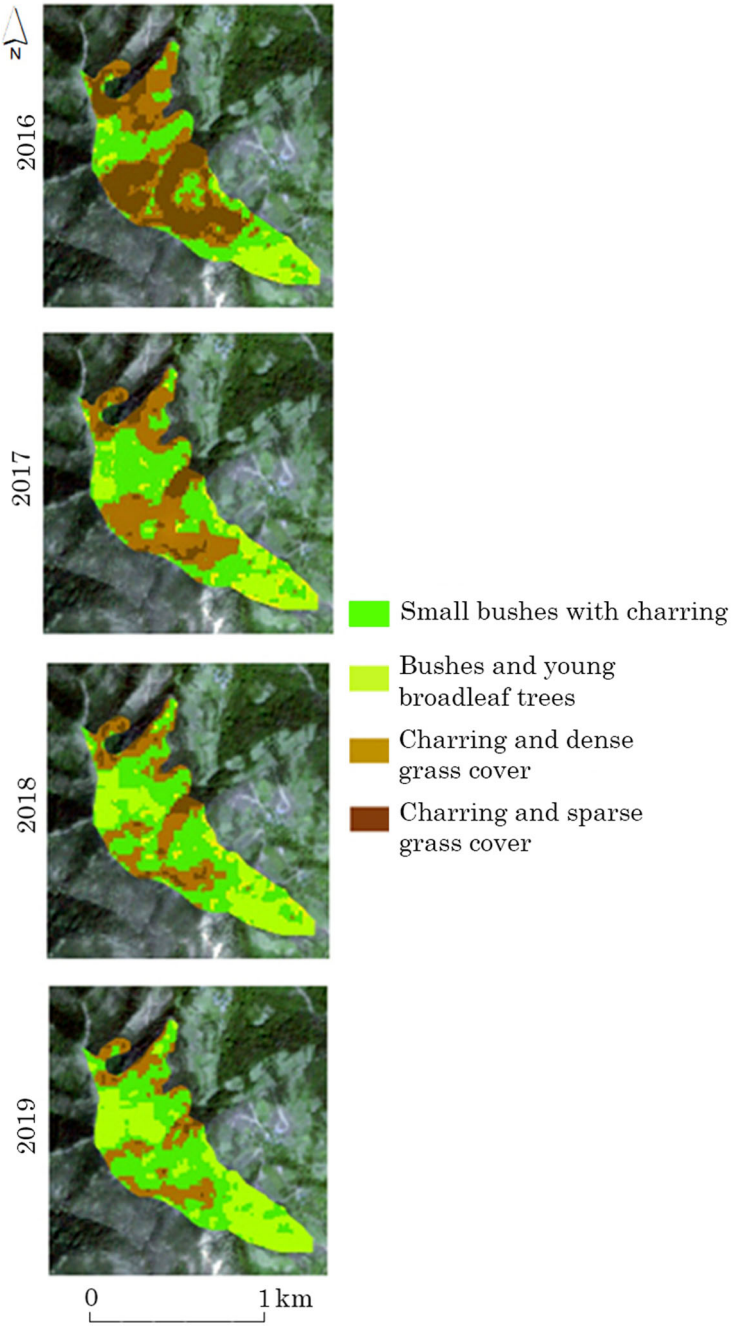

Figure 8. Classification results for study site 3.

capabilities (Eva and Lambin 1998). Although Brightness and Wetness indices revealed long-term effects of fire in vegetated land (Eva and Lambin 1998), class separability by most of tested vegetation indices already was generally poor after one post-fire growing season. Meanwhile, BAIS2 separated burnt forest area after as many

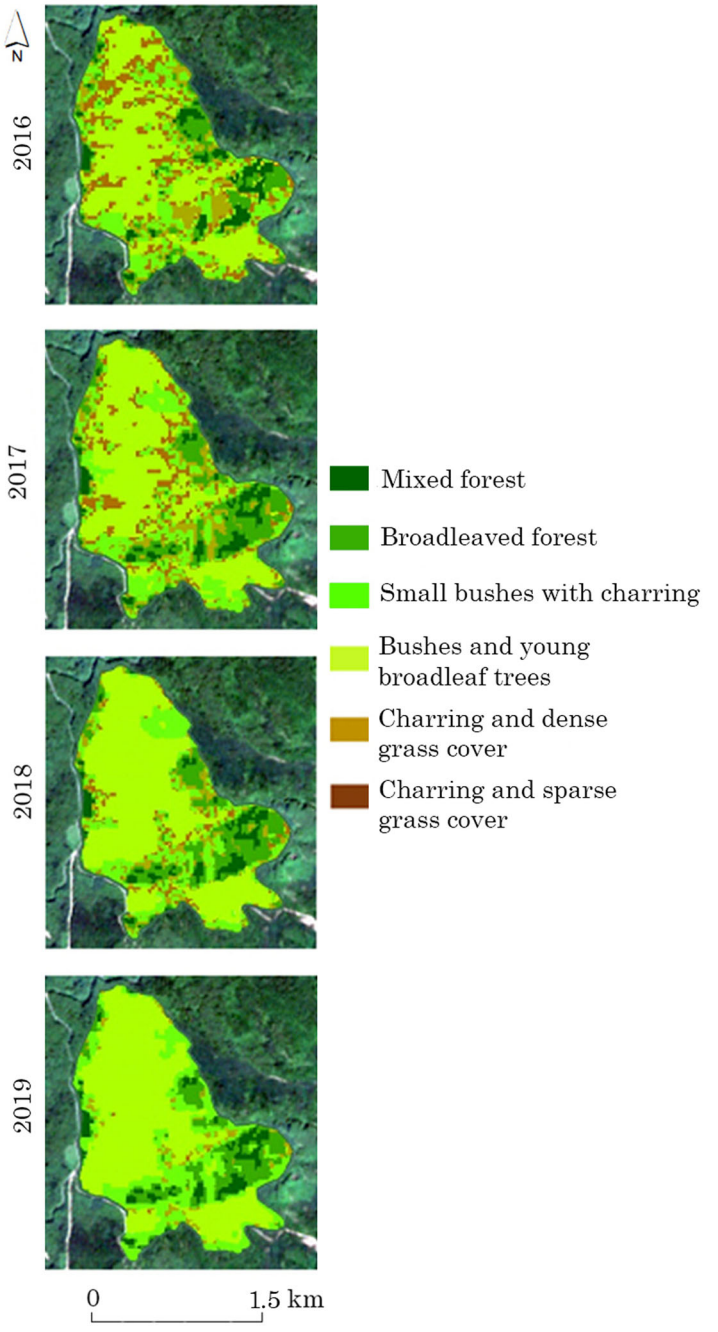

Figure 9. Classification results for study site 4.

as nine post-fire growing seasons in our study. Our result demonstrated a stability of BAIS2 to identify a burnt area independently to vegetation period of satellite data acquisition.

Table 4. Confusion matrices resulting from classifying test pixels.

a) Study site 1

	Small bushes with charring	Charring with dense grass cover	Forest	Row total
Small bushes with charring	**705**	18	91	814
Charring with dense grass cover	2	**129**	1	132
Forest	54	7	**194**	255
Column total	761	154	286	1201

Classification input is Sentinel-2 bands, BAIS2 and texture (2019).

b) Study site 2

	Bushes and young broadleaf trees	Small bushes with charring	Charring and sparse grass cover	Charring and dense grass cover	Forest	Row total
Bushes and young broadleaf trees	**2867**	822	0	9	91	3789
Small bushes with charring	806	**2752**	3	6	85	3652
Charring and sparse grass cover	1	0	**399**	4	0	404
Charring and dense grass cover	53	25	417	**1313**	11	1819
Forest	9	224	0	2	**812**	1047
Column total	3736	3823	819	1334	999	10,711

c) Study site 3

	Bushes and young broadleaf trees	Small bushes with charring	Charring and sparse grass cover	Charring and dense grass cover	Row total
Bushes and young broadleaf trees	**846**	141	0	20	1007
Small bushes with charring	149	**703**	12	18	882
Charring and sparse grass cover	11	3	**182**	7	203
Charring and dense grass cover	0	4	8	**49**	61
Column total	1006	851	202	94	2153

d) Study site 4

	Bushes and young broadleaf trees	Small bushes with charring	Charring and sparse grass cover	Charring and dense grass cover	Forest mixed	Forest broadleaf	Row total
Bushes and young broadleaf trees	**131**	25	0	0	7	8	169
Small bushes with charring	224	**2031**	0	3	12	86	2356
Charring and sparse grass cover	8	0	**158**	23	0	2	191
Charring and dense grass cover	16	1	21	**171**	4	0	213
Forest mixed	12	13	0	5	**162**	35	227
Forest broadleaf	0	26	3	7	201	**1287**	1524
Column total	391	2096	182	209	386	1416	4680

The diagonal elements (bold) represent the number of points for which the predicted label is equal to the true label, while off-diagonal elements are those that are mislabelled by the classifier.

4.3. Classification of burnt forest areas

The success of classification is determined by its ability to identify the feature of an object that is most useful for that object's discrimination. Study sites were classified

Table 5. Classification accuracy.

Accuracy measure	Study site	S2 bands	S2 bands with BAIS2	S2 bands with BAIS2 and texture FT	S2 bands with BAIS2 and texture S
Overall accuracy	1	0.72	**0.76**	0.75	0.74
	2	0.74	0.77	**0.83**	0.81
	3	0.75	0.80	**0.86**	0.83
	4	0.69	**0.78**	**0.78**	0.77
Kappa coefficient	1	0.68	**0.74**	0.72	0.72
	2	0.72	0.75	**0.80**	0.80
	3	0.73	0.78	**0.84**	0.80
	4	0.67	**0.77**	**0.77**	0.76

Bold values indicate the highest accuracy measure for specific study site.
S2 is Sentinel-2 image, BAIS2 is Burned Area Index for Sentinel-2, FT is texture by Fourier transform, S is texture by image statistics computation.

for four (study site 1, study site 3), five (study site 2) and six (study site 4) classes. Overall accuracy ranged from 0.69 to 0.86 and Kappa coefficient from 0.67 to 0.84, depending on input features used in classification (Table 5).

In general, our results are comparable with those from recent studies. Mitri and Gitas (Trigg and Flasse 2000) separated five classes in burnt forest areas on the Greek island of Thasos 14 and 18 years after fire from Hyperion satellite image using an object-based classification approach. Those classes were '*brutia* mature', '*nigra* mature', '*brutia* regeneration', '*nigra* regeneration' and 'other vegetation'. Applying an object-based classification from SPOT and ERS satellite images for the island of Thasos, Polychronaki *et al.* (Fornacca et al. 2018) assessed overall accuracy to be 0.76 and Kappa coefficient 0.69. Post-fire land covers were mapped with 0.90 overall accuracy and 0.84 Kappa coefficient. Four land cover types (low-vegetation, artificial areas and bare land, broadleaf, and mixed class with shrubs and trees) were classified on burnt forest areas 19 and 23 years after fire.

In detail, the classification from our study based on satellite S2 spectral bands revealed the lowest overall accuracy (from 0.69 to 0.75) and Kappa coefficients (from 0.67 to 0.73) for all study sites. Stronger results were demonstrated for classification based on combination of S2 bands and BAIS2, where overall accuracy ranged from 0.76 to 0.80 and Kappa coefficient from 0.74 to 0.78. Approaches using S2 spectral bands in combination with various vegetation indices (e.g. NBR, BAIS2, Mid Infrared Burn Index [MIRBI]) were successfully used in identification of burnt forest areas in Italy (Meng et al. 2017) and in distinguishing burnt pixels in Sub-Saharan Africa (Roteta et al. 2019). These studies, however, identified burnt forest areas without further classification of land cover types inside a burn. From our knowledge, we have identified only two recent publications describing use of Landsat or S2 spectral index approaches for estimating burn severity inside burnt area (Fernández-Manso et al. 2016; Fornacca et al. 2018). Burn-severity discrimination was classified into four severity levels from S2 red-edge spectral indices after vegetation wildfire in Spain (Fernández-Manso et al. 2016). While spectral index approaches applied for estimating burn severity in Greece using Normalized Difference Moisture Index (NDVI), Normalized Difference Moisture Index (NDMI), and Normalized Burn Ratio (NBR) from Landsat TM data were indicated to contain inaccuracies, a revised index design

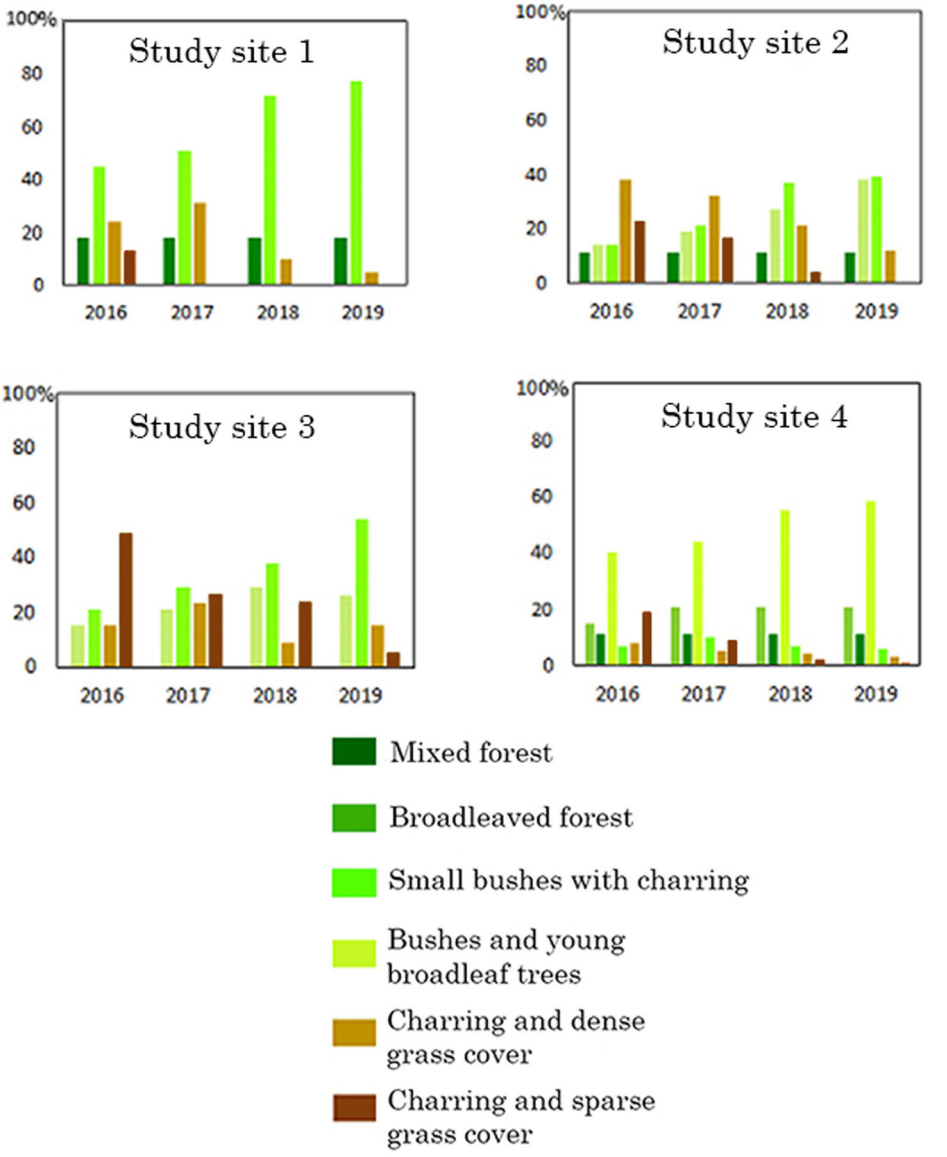

Figure 10. Dynamic in study site land covers.

or alternative methods could improve the estimation of burn severity (Mitri and Gitas 2010).

Classification based on combination of S2 bands, BAIS2, and texture by Fourier transform was the most accurate in our study and showed the best results for study site 2 (overall accuracy of 0.83 and Kappa coefficient of 0.80) and for study site 3 (overall accuracy of 0.86 and Kappa coefficient of 0.84). The relatively high classification accuracy for study site 2 can be explained by its being the largest area (188.5 ha) among the four. The texture algorithm worked more effectively here due to the presence of more 16×16 window size pixels for texture analysis. In the case of study site 3, classification accuracy results can be explained by the greater difference in texture of charring with

grass cover due to the high fire danger class (Table 1) that serves as a proxy of fire intensity in our study. Study site 4 was classified with equal accuracy using two sets of classification inputs: S2 bands, BAIS2, and texture by Fourier transform; as well as S2 bands and BAIS2 (overall accuracy of 0.78, Kappa of 0.77). This may be a consequence of too-small differences in texture within burn land covers 9 years after fire, and these were not sensitive to the proposed Fourier transform method.

Adding the texture by image statistic computation into a combination of S2 bands and BAIS2 either reduced the classification accuracy (as measured by overall accuracy for all study sites) or left the accuracy unchanged (as seen in the Kappa coefficient for study sites 1 and 2) compared to classification results when adding the texture by Fourier transform. Similarly, statistical texture features indicated lower overall accuracy (0.87) and Kappa coefficient (0.83) compared to classification using grey level co-occurrence matrix as the texture feature (0.92 and 0.87, respectively) in land cover classification from QuickBird image with Support Vector Machine classifier (Polychronaki et al. 2014).

Based on our findings, study site area and post-fire period influence on the classification accuracy when texture feature is applying. Generally, the classification of land covers in the study sites while including texture feature was more accurate than was classification without texture feature. This finding is in accordance with results from recent research by Kupidura (Kupidura 2019), where the efficiency of selected texture features was shown in the process of land use land cover RF (random forest) classification from satellite S2 data. Classification with texture analysis from our study were less accurate (overall accuracy ranging from 0.78 to 0.86 and Kappa coefficient from 0.77 to 0.83) than classification with texture analysis from Kupidura (Kupidura 2019) overall accuracy ranging from 0.92 to 0.97 and Kappa coefficient from 0.90 to 0.96), where textural differences of land cover classes were greater.

4.4. Dynamics in land cover classes of study sites

Dynamics in land cover classes of study sites are demonstrated in bar charts (Figure 10). Natural regeneration of pine was not observed on study sites, even though sites 1, 2, and 3 had been dominated by Austrian pine before the fire. Establishment of coniferous species plantations in areas naturally dominating by deciduous broadleaf forests was a widely used practice in Serbia in the past (Tomić et al. 2011) as it was the case on our study area. However, the indigenous vegetation on the sites are oaks (Table 1) and this might be the reason for the observed better regeneration of broadleaf species. Also, it is known that broadleaf species have post-fire ecological strategies, such as re-sprouting ability, which is a key trait to overcome such disturbances as fires (Clarke et al. 2013). According to Mekonnen *et al.* (Mekonnen et al. 2019), rapid nitrogen mineralization after fire might be more beneficial for the broadleaf than coniferous tree species in the first 5 years after fire.

The intensity of vegetation recovery after a fire obviously relates to fire intensity (fire danger class), burn severity, time elapsed since the fire and area of burnt. Specifically, the higher fire intensity, the more time is needed for vegetation recovery (Clarke et al. 2013; Mekonnen et al. 2019). This can be well documented by the

vegetation dynamics in our study sites. Study site 1 had the greatest increase in small bushes with charring class compared to the other sites for the study period. This site was 6 years post fire and its fire danger class indicating fire intensity was very high. The dynamic results of study site 1 confirmed findings from similar studies, where recovery was greater for higher severity areas and vegetation recovery dynamics were generally greatest for several years following fire (Epting and Verbyla 2005, Bright et al. 2019). In contrast, recovery at study site 2 was much slower compared to in study site 1, even though the fire events at both occurred in the same year, 2012. Site recovery dynamics following forest fires are strongly influenced by the area burned by fire, type of vegetation burnt, neighboring vegetation type, and post-fire recovery time (Viana-Soto et al. 2017). The study site 2 is seven times larger than study site 1, and therefore the effect of surrounding unburnt vegetation on the recovery process is much weaker (Nathan and Muller-Landau 2000). In addition, southern slopes with drier conditions contribute to slower regeneration (Cai et al. 2013) and neighboring with burn conifer vegetation contributes to slower regeneration of burnt vegetation (Liu 2016).

Study site 3 had the largest proportion of charring with sparse grass cover class among all sites for the study period. That was due to the shorter post-fire period according to the date of the satellite data analysis (1 year after fire). This can be explained by high representation of grasses and herbaceous species, which usually appear first and recover quickly following the 'mineral flush' that occurs after fire (Christensen 1994). Study site 4 had little presence of charring with sparse grass cover class due to overgrowing vegetation by the date of the satellite data analysis (9 years after fire).

The fire impact categories can be assigned based on our study findings to describe the forest ecosystem response after fire from satellite data: minor (class forest), minor to moderate (class bushes with young broadleaf trees), moderate (class small bushes with charring), moderate to strong (class charring with dense grass cover) and strong (class charring with sparse grass cover). The suggested fire impact categories potentially can improve assessment of fire effects from forest inventory.

The information regarding post-fire vegetation dynamics in the study sites can be useful for continuous monitoring and assessment of forest succession. Hence, the method can support planning of forest measures to aid in effective restoration of forest cover after fire events.

5. Conclusions

The proposed method for monitoring post-fire forest scars combined spectral and textural features of land cover types *inside* a post-fire study sites. The optimal feature combination for mapping post-fire land cover types was investigated. Stability of BAIS2 index within the analysed May-September vegetation period was tested.

Our study revealed that classification results were significantly improved by taking into consideration the texture of burnt forest area. The most accurate classification method for characterizing study sites was based on a combination of Sentinel-2 bands, BAIS2, and texture by Fourier transform. This methodological approach was

successfully tested to assess vegetation recovery in contrasting post-fire study sites. The proposed method can be considered as an improvement of recent studies classifying the post-fire scars. The method could be applied also to burnt areas in temperate zone and can help in assessing vegetation response after fire and aid restoration efforts. The study and findings can support planning of forest management measures needed to effectively restore forest cover.

Disclosure statement

The authors declare no conflict of interest.

Funding

This research was funded by the Ministry of Education, Youth and Sports of the Czech Republic within the National Programme for Sustainability I (grant LO1415). The study fields work was supported financially by the Ministry of Education, Science and Technological Development of the Republic of Serbia, grant number 451-02-68/2020/14/2000169 for financing scientific research at the Faculty of Forestry University of Belgrade in 2020.

Data availability statement

The data that support the findings of this study are available on request from the corresponding author, OB.

References

Aleksić P, Krstić M, Jančić G. 2009. Forest fires – ecological and economic problem in Serbia. Bot Serbica. 33(2):169–176.

Banković S, Medarević M, Pantić D, Petrović N. 2008. Nacionalna Inventura Šuma Republike Srbije. Šumarstvo (Forestry). 3:1–16.

Banskota A, Kayastha N, Falkowski MJ, Wulder MA, Froese RE, White JC. 2014. Forest monitoring using landsat time series data: a review. Can J Remote Sens. 40 (5):362–384.

Bekkari A, Idbraim S, Elhassouny A, Mammass D, El Yassa M, Ducrot D. 2012. SVM and Haralick features for classification of high resolution satellite images from urban areas. In: Elmoataz A, Mammass D, Lezoray O, Nouboud F, Aboutajdine D, editors. ICISP 2012, Berlin (Germany): Springer; p. 17–26.

Bracewell RN. 2000. The Fourier transform and applications. McGraw Hil, Morgan & Claypool Publishers, California, USA.

Bright BC, Hudak AT, Kennedy RE, Braaten JD, Henareh Khalyani A. 2019. Examining post-fire vegetation recovery with landsat time series analysis in three Western North American forest types. Fire Ecol. 15 (1):8.

Cai W, Yang J, Liu Z, Hu Y, Weisberg PJ. 2013. Post-fire tree recruitment of a Boreal Larch forest in Northeast China. For Ecol Manage. 307:20–29.

Christensen NL. 1994. The effects of fire on physical and chemical properties of soils in Mediterranean-climate shrublands. In: Moreno JM, Oechel WC, editors. The role of fire in Mediterranean-type ecosystems; Springer-Verlag, New York Inc, p. 79–95.

Chu T, Guo X, Chu T, Guo X. 2013. Remote sensing techniques in monitoring post-fire effects and patterns of forest recovery in Boreal forest regions: a review. Remote Sens. 6 (1): 470–520.

Clarke PJ, Lawes MJ, Midgley JJ, Lamont BB, Ojeda F, Burrows GE, Enright NJ, Knox KJ. 2013. Resprouting as a key functional trait: how buds, protection and resources drive persistence after fire. New Phytol. 197 (1):19–35.
Cristianini N, Shawe-Taylor J. 2000. An introduction to support vector machines and other kernel-based learning methods. Cambridge University Press, The Edinburgth Building, Cambridge, CB2 2RU, UK.
Cuevas-Gonzalez M, Gerard F, Balzter H, Riaño D. 2009. Analysing forest recovery after wildfire disturbance in Boreal Siberia using remotely sensed vegetation indices. Glob Change Biol. 15(3):561–577.
Díaz-Delgado R, Lloret F, Pons X. 2003. Influence of fire severity on plant regeneration by means of remotesensing imagery. Int J Remote Sens. 24(8):1751–1763.
Dowdy AJ, Mills GA, Finkele K, de Groot W. 2009. Index sensitivity analysis applied to the Canadian Forest Fire Weather Index and the McArthur Forest Fire Danger Index. Meteorol Appl. 17: 298–312.
Epting J, Verbyla D. 2005. Landscape-level interactions of prefire vegetation, burn severity, and postfire vegetation over a 16-year period in interior Alaska. Can J For Res. 35(6): 1367–1377.
Eva H, Lambin EF. 1998. Remote sensing of biomass burning in tropical regions. Remote Sens Environ. 64 (3):292–315.
Fernández-Manso A, Fernández-Manso O, Quintano C. 2016. SENTINEL-2A red-edge spectral indices suitability for discriminating burn severity. Int J Appl Earth Obs Geoinf. 50: 170–175.
Filipponi F. 2018. BAIS2: Burned Area Index for Sentinel-2. Proceedings. 2 (7):364.
Filipponi F. 2019. Exploitation of Sentinel-2 time series to map burned areas at the national level: a case study on the 2017 Italy wildfires. Remote Sens. 11 (6):622.
Fornacca D, Ren G, Xiao W. 2018. Evaluating the best spectral indices for the detection of burn scars at several post-fire dates in a mountainous region of Northwest Yunnan, China. Remote Sens. 10(8):1196.
Gonzales R, Woods R. 1992. Digital image processing. Addison-Wesley Publishing Company, Boston, England.
Haralick RM, Shanmugam K, Dinstein I. 1973. Textural features for image classification. IEEE Trans Syst Man Cybern. 4:610–621.
Huang H, Roy D, Boschetti L, Zhang H, Yan L, Kumar S, Gomez-Dans J, Li J. 2016. Separability analysis of Sentinel-2A multi-spectral instrument (MSI) data for burned area discrimination. Remote Sens. 8 (10):873.
International Forest Fires News (IFFN). International Forest Fires News. 2020. [accessed March 12, 2020]. https://gfmc.online/wp-content/uploads/09-IFFN-37-Serbia-1.pdf.
Kontoes CC, Poilvé H, Florsch G, Keramitsoglou I, Paralikidis S. 2009. A comparative analysis of a fixed thresholding vs. a classification tree approach for operational burn scar detection and mapping. Int J Appl Earth Obs Geoinf. 11(5):299–316.
Koutsias N, Xanthopoulos G, Founda D, Xystrakis F, Nioti F, Pleniou M, Mallinis G, Arianoutsou M. 2013. On the relationships between forest fires and weather conditions in Greece from long-term national observations (1894-2010). Int J Wildland Fire. 22 (4): 493–507.
Kupidura P. 2019. The comparison of different methods of texture analysis for their efficacy for land use classification in satellite imagery. Remote Sens. 11(10), 1233.
Lentile LB, Holden ZA, Smith AMS, Falkowski MJ, Hudak AT, Morgan P, Lewis SA, Gessler PE, Benson NC. 2006. Remote sensing techniques to assess active fire characteristics and post-fire effects. Int J Wildland Fire. 15 (3):319.
Liu Z. 2016. Effects of climate and fire on short-term vegetation recovery in the Boreal larch forests of Northeastern China. Sci. Rep. 6(1):37572.
Lukić T, Marić P, Hrnjak I, Gavrilov MB, Mladjan D, Zorn M, Komac B, Milošević Z, Marković SB, Sakulski D, et al. 2017. Forest fire analysis and classification based on a Serbian case study. Acta Geogr Slov. 57 (1):51–63.

Main-Knorn M, Pflug B, Louis J, Debaecker V, Müller-Wilm U, Gascon F. 2017. Sen2Cor for Sentinel-2. Proceedings Volume 10427, Image and Signal Processing for Remote Sensing XXIII; 1042704 (2017) https://doi.org/10.1117/12.2278218 Event: SPIE Remote Sensing, 2017, Warsaw, Poland.

Marčeta M, Milanović K. 2018. Indicator state and analysis of damage to forest fires on the Territory of the Republic of Serbia for the period from 2012-2016 years. Zb PMF Geog Inst Beograd. 66(66-2):105–119.

Mason JC, Handscomb DC. 2002. Chebyshev polynomials, Chapman and Hall/CRC, New York.

Mekonnen ZA, Riley WJ, Randerson JT, Grant RF, Rogers BM. 2019. Expansion of high-latitude deciduous forests driven by interactions between climate warming and fire. Nat Plants. 5 (9):952–958.

Mencuccini M, Christoffersen B. 2019. Modelling water fluxes in plants: from tissues to biosphere. New Phytol. 222(3):1207–1222.

Meng R, Wu J, Schwager KL, Zhao F, Dennison PE, Cook BD, Brewster K, Green TM, Serbin SP. 2017. Using high spatial resolution satellite imagery to map forest burn severity across spatial scales in a Pine Barrens ecosystem. Remote Sens Environ. 191:95–109.

Milanović S. 2019. The improvement of the forest fire protection system in the Republic of Serbia. [accessed August 30, 2019]. https://upravazasume.gov.rs/domaci-projekti/.

Milne AK. 1986. The use of remote sensing in mapping and monitoring vegetational change associated with bushfire events in Eastern Australia. Geocarto Int. 1(1):25–32.

Mitri GH, Gitas IZ. 2010. Mapping postfire vegetation recovery using EO-1 Hyperion imagery. IEEE Trans Geosci Remote Sens. 48 (3):1613–1618.

Moreira F. 2012. Post-fire management and restoration of Southern European forests. Springer. Science, Business Media B.V.

Moriondo M, Good P, Durao R, Bindi M, Giannakopoulos C, Corte-Real J. 2006. Potential impact of climate change on fire risk in the Mediterranean area. Clim Res. 31 (1):85–95.

Morresi D, Vitali A, Urbinati C, Garbarino M. 2019. Forest spectral recovery and regeneration dynamics in stand-replacing wildfires of Central Apennines derived from landsat time series. Remote Sens. 11(3):308.

Nathan R, Muller-Landau HC. 2000. Spatial patterns of seed dispersal, their determinants and consequences for recruitment. Trends Ecol E. 15 (7):278–285.

Patterson MW, Yool SR. 1998. Mapping fire-induced vegetation mortality using landsat thematic mapper data: a comparison of linear transformation techniques. Remote Sens Environ. 65(2): 132–142.

Polychronaki A, Gitas IZ. 2010. The development of an operational procedure for burned-area mapping using object-based classification and ASTER imagery. Int J Remote Sens. 31 (4): 1113–1120.

Polychronaki A, Gitas IZ, Minchella A. 2014. Monitoring post-fire vegetation recovery in the Mediterranean using SPOT and ERS imagery. Int J Wildland Fire. 23 (5):631.

Proisy C, Couteron P, Fromard F. 2007. Predicting and mapping mangrove biomass from canopy grain analysis using fourier-based textural ordination of IKONOS images. Remote Sens Environ. 109 (3):379–392.

Radovanovic M, Pavlovic T, Stanojevic G, Milanovic M, Pavlovic M, Radivojevic A. 2015. The influence of solar activities an occurrence of the forest fires in South Europe. Therm Sci. 19 (2):435–446.

Ratknić T. 2017. Analysis of the profitability of the restitution of fire-affected beech forests in Serbia. Appl Ecol Env Res. 15(4):1999–2010.

Roteta E, Bastarrika A, Padilla M, Storm T, Chuvieco E. 2019. Development of a Sentinel-2 burned area algorithm: generation of a small fire database for Sub-Saharan Africa. Remote Sens Environ. 222:1–17.

Ryu JH, Han KS, Hong S, Park NW, Lee YW, Cho J. 2018. Satellite-based evaluation of the post-fire recovery process from the worst forest fire case in South Korea. Remote Sens. 10 (6):918.

San-Miguel-Ayanz J, Branco A, Pfeiffer H, Vivancos TA, Nuitjen D, Libertà G, Maianti P, Boca R, De Rigo D, Ferrari D, Durrant T. 2019. Forest fires in Europe, Middle East and North Africa. doi:978-92-76-11234-1.

Teodoro A, Amaral A. 2019. A statistical and spatial analysis of Portuguese forest fires in summer 2016 considering Landsat 8 and Sentinel 2A data. Environments. 6(3):36.

Tomic Z, Rakonjac L, Isajev V. 2011. The selection of species for reforestation and amelioration in Central Serbia.Belgrade: Institute of Forestry, Belgrade: 232. [in Serbian]. Available at: https://www.forest.org.rs/pdf/Monografija_2011_Izbor_vrsta_za_po%C5%A1umljavanje_i_melioracije_u_centralnoj_Srbiji.pdf

Trigg S, Flasse S. 2000. Characterizing the spectral-temporal response of burned Savannah using in situ spectroradiometry and infrared thermometry. Int J Remote Sens. 21 (16): 3161–3168.

Turco M, Llasat MC, von Hardenberg J, Provenzale A. 2014. Climate change impacts on wildfires in a Mediterranean environment. Clim Change. 125 (3-4):369–380.

van der Linden S, Rabe A, Held M, Jakimow B, Leitão P, Okujeni A, Schwieder M, Suess S, Hostert P. 2015. The EnMAP-box—a toolbox and application programming interface for EnMAP data processing. Remote Sens. 7 (9):11249–11266.

Veraverbeke S, Somers B, Gitas I, Katagis T, Polychronaki A, Goossens R. 2012. Spectral mixture analysis to assess post-fire vegetation regeneration using landsat thematic mapper imagery: accounting for soil brightness variation. Int J Appl Earth Obs Geoinf. 14 (1):1–11.

Viana-Soto A, Aguado I, Martínez S. 2017. Assessment of post-fire vegetation recovery using fire severity and geographical data in the Mediterranean region (Spain). Environments. 4 (4):90.

Vogelmann JE, Gallant AL, Shi H, Zhu Z. 2016. Perspectives on monitoring gradual change across the continuity of landsat sensors using time-series data. Remote Sens Environ. 185: 258–270.

White J, Ryan K, Key C, Running S. 1996. Remote sensing of forest fire severity and vegetation recovery. Int J Wildland Fire. 6(3):125.